Atmósfera (1996), **9**, *pp. 1-21*

Comparison of temporal cloud variability simulated by a GCM with observations from the Nimbus–7 Satellite

AMADOR ARGETE[1] and IAN SIMMONDS[2]

Department of Meteorology and Oceanography, College of Science
University of the Philippines, Diliman, Quezon City, Philippines 1101

(Manuscript received Feb. 17, 1995; accepted in final form June 12, 1995)

RESUMEN

Este trabajo describe la variabilidad temporal de la nubosidad a partir de observaciones provenientes del satélite Nimbus-7 y una simulación del GCM. Las nubes de la simulación son parametrizadas mediante la función de distribución cumulativa normal para relacionar cantidades fraccionales de nubes con la humedad relativa de gran escala. Se presentan las distribuciones globales de las características nubosas de ambas fuentes de datos incluyendo sus promedios y desviaciones estándares temporales. Para las observaciones del Nimbus-7 los periodos son para los meses DEF y JJA, 1979-1985 mientras que los datos simulados corresponden a eneros y julios perpetuos. Las varianzas contribuidas por las fluctuaciones con periodos entre 2.5 a 6.0 días y 10 días son extraídas.

Ambos campos, el observado y el simulado de variabilidad nubosa muestran una fuerte dependencia zonal. Las fluctuaciones de alta frecuencia son predominantes en las latitudes medias, mientras que las de baja frecuencia prevalecen en los trópicos y en las regiones polares. En general, las variabilidades nubosas no filtradas son mayores en las regiones asociadas con la ciclólisis.

El modelo de GC funciona muy bien, no sólo al simular las medias estacionales, sino también las variabilidades en las bandas temporales examinadas.

Se dan, asimismo, algunas razones para las configuraciones de variabilidad nubosa extraída, en lugares diversos y con diferentes alturas de nubes.

ABSTRACT

This paper describes temporal cloudiness variability from Nimbus-7 satellite observations and a GCM simulation. The GCM clouds are parameterized using the cumulative normal distribution function to relate fractional cloud amount with large-scale relative humidity. The global distributions of cloudiness characteristics from both data sources are presented, including their temporal means and standard deviations. For the Nimbus-7 observations, the periods are for DJF and JJA, 1979-1985 while the simulated data are for perpetual January and July. Variances contributed by fluctuations with periods between 2.5 to 6 days, and >10 days are extracted.

Both observed and simulated cloud variability fields show strong zonal dependence. High-frequency fluctuations are more predominant in the middle latitudes while low-frequency fluctuations predominate in the tropics and the polar regions. In general, unfiltered cloud variabilities are highest in regions associated with cyclolysis. The GCM performs creditably in not only simulating the seasonal means but also the variabilities in the temporal bands examined. Some reasons for the extracted cloud variability patterns at different locations and for different cloud heights are given.

---

[1] Presently at Max-Planck-Insitut für Meteorologie, Bundesstrasse 55, 20146 Hamburg, Germany

[2] School of Earth Sciences, University of Melbourne, Parkville, Victoria, Australia 3052

1. Introduction

Significant progress has been made in the incorporation of interactive cloudiness in General Circulation Models (GCMs). Over the past two decades the treatment and parameterization of clouds have been steadily made better as chronological reference to the papers of Kasahara and Washington (1971), Sasamori (1975), Geleyn (1981), Tiedtke (1985), Slingo (1985), Saito and Baba (1988), and Xu and Krueger (1991) will show. These diagnostic parameterizations of cloudiness in climate models have resulted in close approximations of the observed climatological cloud fields. Although the coarse resolutions of present GCMs precluded the inclusion of more involved cloud physics in the parameterization schemes, such interactive cloudiness has markedly improved the performance of climate models. This is primarily because cloud-related processes are very important in determining the climatic state and that the incremental change in the radiative balances is significantly improved with temporally variable cloudiness fields (Slingo, 1987).

In assessing the suitability of an interactive cloud parameterization scheme in a GCM, it is the usual practice to compare cloud observations with the simulation results. The comparison is often confined to zonally averaged cloudiness patterns as well as the spatial distributions of mean cloud fields at different levels (Hughes, 1984). Although this is a sufficient test in many climatological applications, such analysis has the potential of missing out on the strongly temporal nature of cloud-radiative forcing (Charlock *et al.*, 1993). A comprehensive assessment of cloud generation in a GCM should include not only an appraisal of the mean cloud fields, but also the extent that the model is able to capture cloud variability in various temporal bands. This is very important because cloud cover is involved in nonlinear time-dependent feedbacks with other atmospheric parameters.

Climate variability is an indirect measure of how benign a particular region's climate is. In the case of cloudiness, variability can also be associated with the variability of other meteorological variables such as rainfall and solar intensity. Together with mean values, it can be used to quantify a particular region's susceptibility to extreme conditions like droughts and prolonged rainfall events. Subject to the availability of longer observational data sets, variability fields can also be used to discern long-term climate trends from baseline climate 'noise'. This application is expected to be of growing importance, considering the unavoidable impact of human activities on the climate system.

The importance of properly simulating the observed spatial distribution of variance and covariance statistics in climate models has long been recognized (Blackmon and Lau, 1980; Katz, 1983; Jones and Simmonds, 1993). Increasingly, the climate community is addressing the question of atmospheric variability, including the structure, and model representations, of synoptic systems. Work done regarding the analysis of spatial and temporal variability patterns of cloudiness is much more recent (Bishop and Rossow, 1991; Morcrette, 1991; Yu *et al.*, 1991; Weare, 1992; Gent and Tribbia, 1993). A reason for this is the difficulty of GCM cloud representation, particularly for low clouds. This latter shortcoming leads to errors in the estimation of shortwave absorption at the surface (Soden, 1992). Nevertheless, coarse resolution GCMs with interactive cloudiness performs well in simulating longwave emission to space.

The regional characteristics of some meteorological fields have been examined, with the significant finding that their temporal variabilities exhibit geographical, usually zonal dependence (Blackmon and Lau, 1980; Jones and Simmonds, 1993). Variabilities at low and high latitudes were seen to be dominated by low frequency modes, while high frequency modes are more prevalent in the middle latitudes, particularly in regions of extratropical storm tracks. Similarly, the low frequency part of OLR variability is dominant in the low-latitudes and has the largest amplitudes over the summer continents (Slingo *et al.*, 1992). This finding is relevant to the effects that

interactive cloudiness have on climate, especially with regards to the intensification of convective instability in the tropics. Since the evolution of all meteorological variables are inherently linked with one another, this paper was prompted by the desire to look at the temporal modes of variability of cloudiness at all levels. The regional characteristics of these second-moment statistics should add to the understanding of transient weather systems. The comparison between modelled and observed cloud variabilities will show the strengths and deficiencies of GCMs, and give an indication on the ability of the cloud parameterization scheme in capturing regional cloudiness characteristics. In particular, the degree of skill to which variability is simulated in different latitude bands may infer some information about the appropriateness of our treatments of clouds associated with, say, tropical convection and midlatitude systems.

2. Data sets and analysis procedures

The model-generated data came from 600-day perpetual January and July simulations using the Melbourne University GCM described by Simmonds (1985) and Simmonds *et al.* (1988). Fractional cloudiness is parameterized using relative humidity as the predictor, the main assumption being the normal distribution of relative humidity over a gridbox. Following the results of observational studies by Ricketts (1973) and Kvamsto (1991), fractional cloudiness varies with relative humidity with the relationship given by the cumulative normal distribution function whose density curve is:

$$f(x) = \frac{1}{\sqrt{2\pi\sigma_c^2}} e^{-\frac{(x-\mu)^2}{2\sigma_c^2}} \tag{1}$$

where μ is the mean, σ_c is the standard deviation and x is the variable of integration. In this formulation, fractional cloudiness is the area under the normal curve from $x = -\infty$ to $x = RH$:

$$C_a = \int_{-\infty}^{x} f(x)dx \tag{2}$$

For every value of relative humidity and μ and σ_c in the parameterization routine, corresponding values of the area under the cumulative normal curve up to and including that RH value are computed. This computed area is the fractional cloudiness of the whole grid.

The value of the mean relative humidity, μ, and standard deviation, σ_c, in the density curve are determined from diagnostic fitting of resultant cloudiness fields with surface cloud observations. The values of both parameters vary with the model's terrain-following sigma level but remain invariant with time. Clouds are generated at six σ levels, with two σ levels for each cloud height. Low clouds are composited using the random overlap assumption from clouds generated at $\sigma = 0.926$ and 0.811, middle clouds from $\sigma = 0.664$ and 0.500, and high clouds from $\sigma = 0.336$ and 0.189. That is, for a cloud level computed from two sigma levels a and b the fractional cloudiness C is:

$$C = 1 - (1 - C_a)(1 - C_b) \tag{3}$$

The total cloudiness fields presented in this paper are similarly composited from cloud amounts at the three cloud levels. Clouds are not allowed to form elsewhere and no method of differentia-

ting cumuliform from stratiform clouds is incorporated in the diagnosis of the resultant cloudiness fields. A limitation of the cloud prediction scheme is the exclusion of cloud formation outside the six σ levels. This removes the possibility of the formation of fog at the lowest σ level and stratospheric clouds at the highest levels.

Observational cloud data for comparison purposes were taken by the Nimbus-7 satellite in the period 1 April 1979 to 31 March 1985. In the climatology to be discussed, the simulations were run with 'twilight' conditions while the Nimbus-7 observations were taken at local noon and midnight, corresponding to the satellite's time of passage. To obtain an appropriate comparison between modelled and observed cloud fields, the satellite observed clouds were analyzed such that the daily values are averages of noon and midnight observations. We discuss below two 'perpetual' month (January and July) simulations with the model. The January simulation was compared with satellite observations for December, January and February, while the July case was compared with observations for June, July and August. The raw satellite data which were in a latitudinally-dependent format (ERB World Grid which divides the Earth into 2070 gridboxes measuring approximately 500 km on each side) were interpolated into a $5^{\circ} \times 5^{\circ}$grid comparable to that of model results.

The relative contributions of the two bands of temporal variability in the series of daily cloud fields were extracted through the use of time filters as defined by Blackmon and Lau (1980). These filters have the form:

$$g_j = a_o[f_j] + \sum_{k=1}^{10} a_k[f_{j+k} + f_{j-k}] \tag{4}$$

where f_j are the unfiltered data at day j, g_j are the filtered values and a_k are the filter coefficients which determine the temporal filtering. The temporal periods considered in this study correspond to synoptic or high frequency (2.5 to 6 days), also called band-pass, and planetary or low-pass (>10 days) timescales. Jones and Simmonds (1993) have used these filters in diagnosing the behavior of mean sea level pressure over the Southern Hemisphere and they show the coefficients which produce these filters.

3. Structure of the mean global cloudiness

The global distribution of time-averaged total cloud cover for January is shown in Figure 1a for the Nimbus-7 observations and in Figure 1b for the GCM simulation. Stippling starts at the 70% contour value. Comparisons between these two cloudiness fields show a correspondence both in terms of magnitude and trend although the model systematically overestimates cloud amounts in areas that are climatologically cloudy, and underestimates cloudiness values otherwise. There is also a good agreement in the general location of cloudiness maxima near the equator and at about 60°N and 60°S, and the cloud minima in the subtropics and near the poles. However, there is a discrepancy in the two patterns in the winter polar zone wherein the model systematically underestimated cloudiness amounts.

Figures 2a and 2b show the corresponding cloudiness patterns for July. The location of tropical cloud maximum is well simulated, including its movement to the summer hemisphere and the observed forking of cloud maximum over East Africa. As in the January case, there is generally an underestimation of cloudiness over climatologically clear regions, and an overestimation in cloudy areas. There is an expected difference between the model generated cloudiness and the satellite observed cloud climatology since the GCM cloud distributions were verified against surface cloud observations (Warren *et al.*, 1986; Hahn *et al.*, 1988). The major differences between

1a

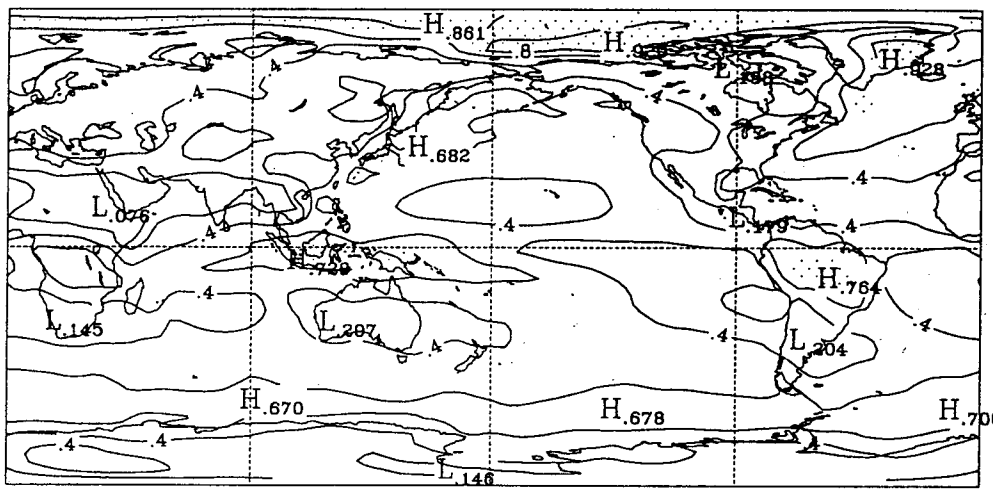

1b

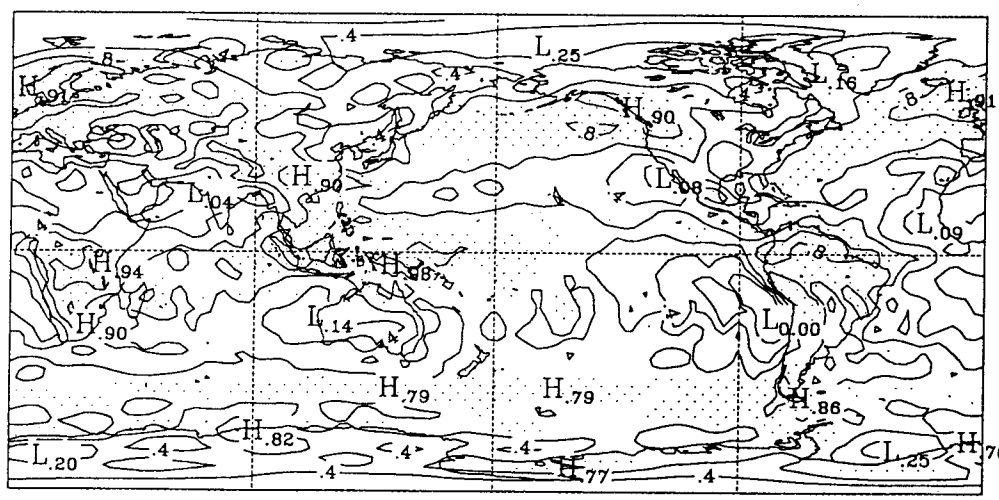

Fig. 1. Time-averaged total clouds for January for a) Nimbus-7 observations and b) GCM simulations. Values above 70% (0.7) are stippled.

the time-mean averages of Nimbus-7 observations and the simulation results, most apparent in the polar regions, are similar to the discrepancies between surface-based and satellite-derived cloudiness values. One reason for the differences between these 'observed' sets is the difficulty in discriminating between low cloud and snow cover, and the paucity of observing stations in the polar regions.

2a

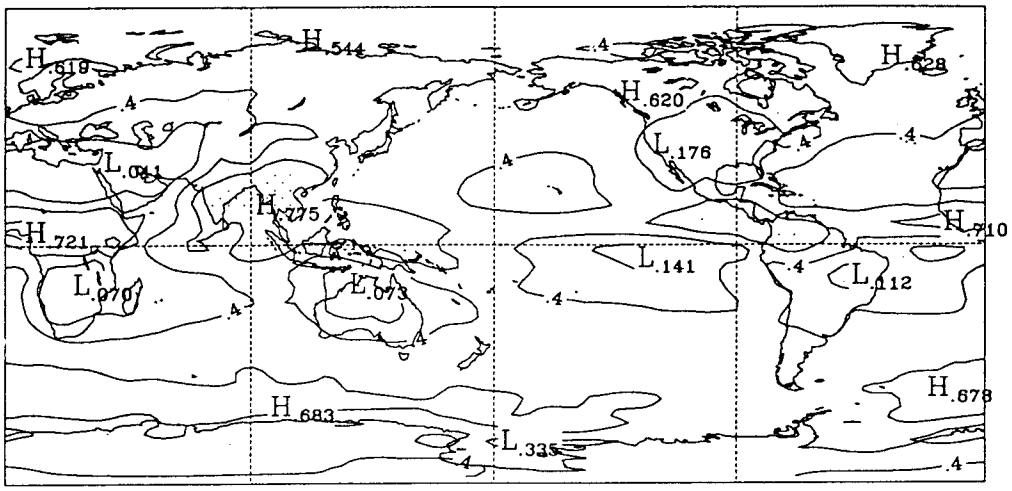

2b

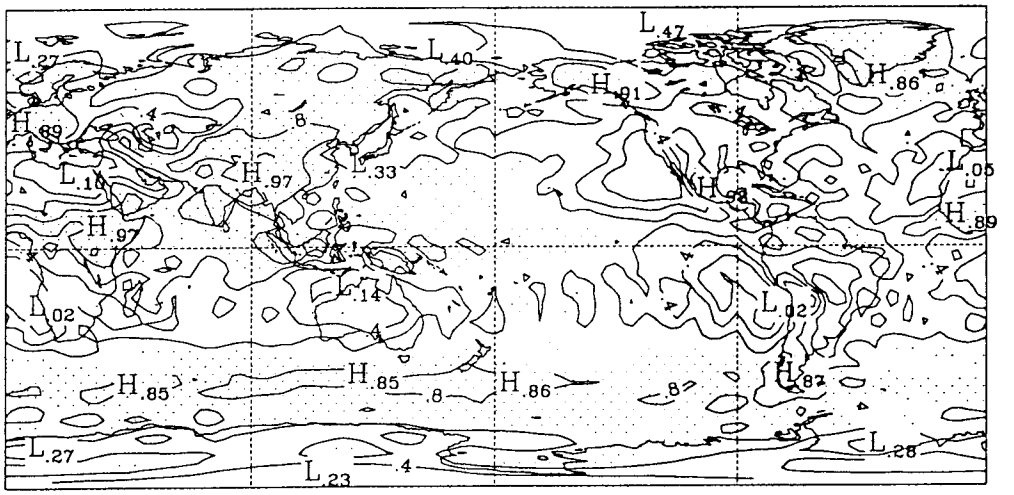

Fig. 2. Time-averaged total clouds for July from a) Nimbus-7 observations and b) GCM simulations. Values above 70% (0.7) are stippled.

A comparison of zonally averaged total clouds for January from surface observations (Warren *et al.*, 1986; Hahn *et al.*, 1988), Nimbus-7, and the simulation is shown in Figure 3a, and in Figure 3b for the July case. Model generated cloudiness amounts fall between the Nimbus-7 and surface observed climatologies except in narrow bands near the subpolar regions of the winter hemisphere. It is apparent that there is a large difference in observed cloud amounts between

3a

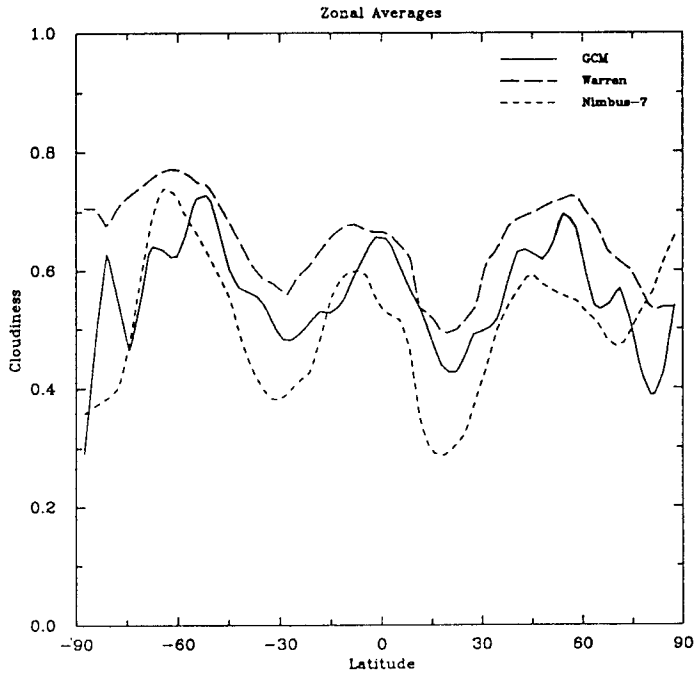

3b

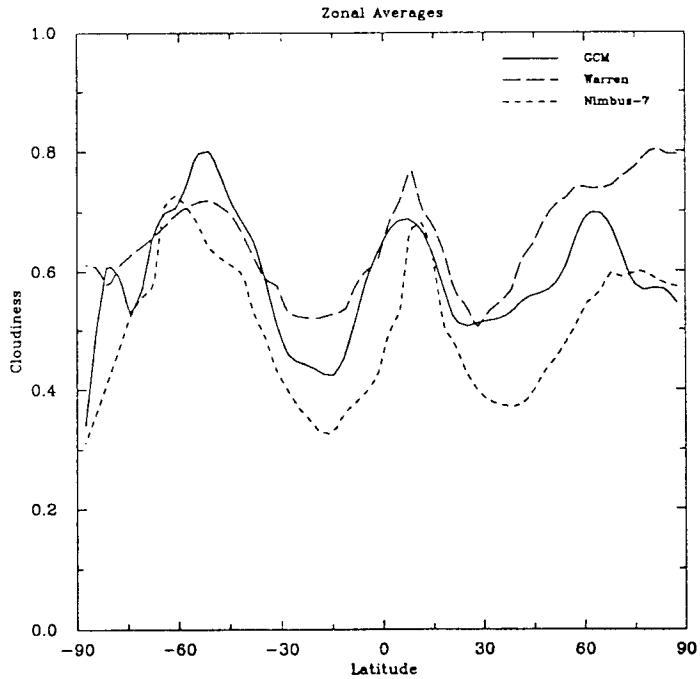

Fig. 3. Zonally-averaged total clouds for a) January and b) July.

the two cloud climatologies considered, especially over the polar regions. Such a wide range of estimates points to biases inherent in cloud observational procedures and the uncertainties as to which 'observed climatology' our simulation results should assume. For surface observations, the difficulty is mainly in the estimation of higher cloud amounts when there are obscuring lower clouds. The reverse is true for satellite cloud observations. Generating cloud values in between the estimates from opposing cloud platforms is deemed sufficient until more data come along, like the ISCCP cloud amounts.

The distributions of model-generated cloudiness are seen to display features generally observed in other cloud climatologies like a) cloudiness maxima at all levels in the ascending branches of the global tricellular circulation; b) cloudiness minima at all levels in the descending branches, c) extensive cloudiness over areas that correspond to low-pressure centers at sea level, and d) extensive cloudiness over warm sea surfaces. The geographical placement and magnitudes of cloudiness are better simulated at higher cloud levels. High clouds are composed of ice particles and are cirriform in nature. Their longer lifetimes contribute to their greater ease in representation in models of the sort used here.

In this study, total cloud amounts have been computed on the assumption that cloudiness at the three cloud levels are overlapping randomly. Aside from being used in the computation of total cloud values, and in getting estimates of cloudiness at levels where cloud amounts can not be determined for various reasons, the concept of cloud overlap is deemed necessary considering the fact that multiple reflections occur between cloud layers and that their effectiveness as radiative modifiers depends on their instantaneous placements (Schneider and Dickinson, 1976). For deep convective clouds, overlap is a fairly straightforward representation but complications set in for shallow clouds. Some authors (Hughes, 1984; Morcrette and Fouquart, 1986; Tian and Curry, 1989) have studied different cloud overlap assumptions at different scales and all reached the conclusion that the random overlap assumption is fairly accurate. Their results indicate one drawback with the random overlap assumption, that is, the systematic underestimation of total cloud amounts by about 5% for grid sizes greater than 90 km. Our results have shown that the isoneph patterns of composited and observed cloudiness fields are strikingly similar although their magnitudes are different. The composited cloud fields systematically underestimated the observed cloud amounts for both seasons, as in Tian and Curry (1989). In addition, the magnitudes of their discrepancies indicate a threshold cloud amount of around 15% below which compositing causes overestimation of observed total cloudiness. At cloud amounts higher than 15%, compositing by random overlap caused observed cloud amounts to be underestimated, the degree of which increases with increasing cloudiness values. Over the convectively active regions of the tropics, the discrepancy was as high as 21%. The sign of this difference is opposite to what might have been expected if the clouds possessed some degree of vertical organization.

If clouds in these convectively active regions are treated as occurring in organized columns, then the composited value should be closer to the observed total as the degree of organization increases. The explanation for the observed discrepancy could be in the treatment of cirrus clouds, the global distributions from the same data source of which are indicative of the patterns and magnitudes of cloud discrepancies. This could mean an undercounting of high cloud amounts systematically occurred in the extraction of cloudiness values at different levels. This is probably because in the Nimbus-7 cloud algorithm, cirrus clouds were analyzed separately from high clouds (Stowe *et al.*, 1989). On the basis of the aforementioned results, random cloud overlap can be considered as a sufficient assumption in the computation of total cloudiness, although care must be observed in the treatment of cloud levels.

4. Observed temporal variability

Figures 4a and 4b show the global distribution of unfiltered standard deviation of observed daily cloudiness for the periods DJF and JJA, 1978 - 1985, respectively. A noticeable feature is the extensive region of high variability over the summer middle latitudes. These regions have climatologically low cloud amounts, implying that the high cloudiness variability is due to convective activity and the formation and dissipation of mesoscale weather systems. Variability is particularly high over the eastern sides of the summer continents and extends well offshore, reflecting the dissipation of cyclones in these climatological high pressure zones. The regions of high cloudiness variability in the subtropical latitudes also coincide with areas associated with tropical cyclolysis, and the peripheries of monsoons. These patterns were most evident in the northwestern and southwestern corners of the Pacific, Indian and Atlantic Oceans, and to a lesser degree in eastern and central parts of the Pacific and Atlantic Oceans. Cloudiness variability is

4a

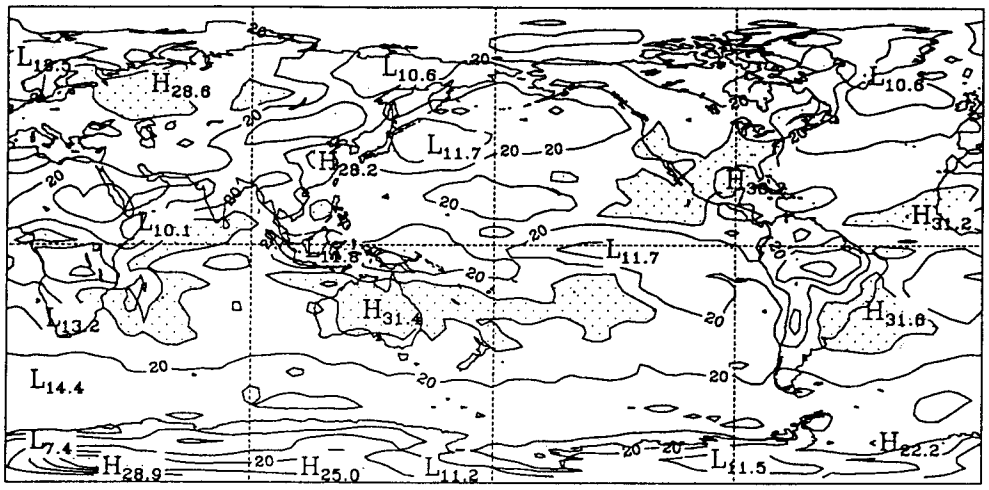

4b

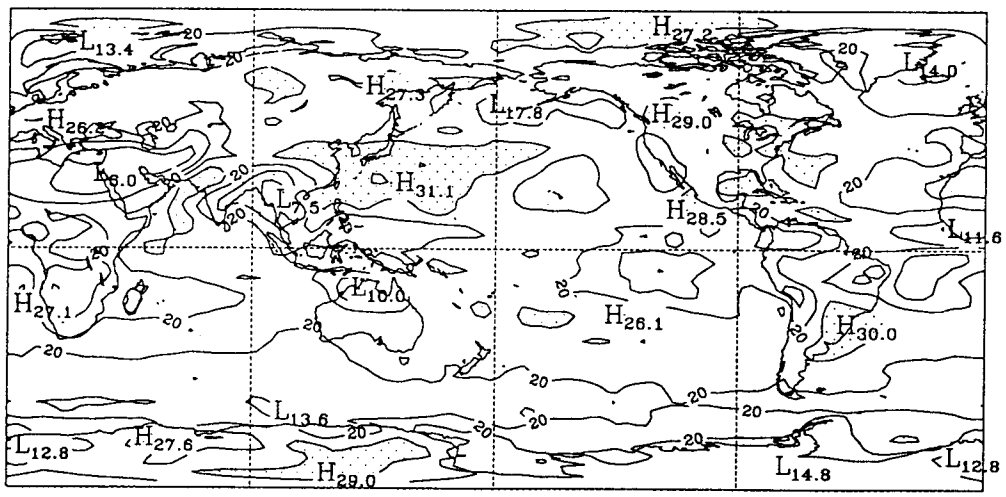

Fig. 4. Unfiltered variabilities of observed cloudiness for a) DJF and b) JJA. Values above 25% are stippled.

always low in the perpetually cloudy regions over the equator and around Antarctica. Likewise, variability is also always low in the climatologically clear areas of North Africa. Cloudiness variability displays a seasonal reversal elsewhere.

Analysis of the variabilities of clouds at different levels (not shown here for brevity) shows a distinctive pattern: high clouds are most variable over the tropics, middle clouds in the middle latitudes, and low clouds in the polar regions. This pattern reflects the different modes of cloud formation at different elevations and latitudes. The variability of high clouds is greatest around the peripheries of the convectively active regions near the equator. The other high-level cloud variability maxima, though of comparatively lower magnitudes, are found in the winter polar regions and assume a three-wave structure. The locations of these variability maxima coincide with the locations of mean sea level pressure variability axes and could be caused by cirrus clouds associated with cyclonic dissipation as they encounter a blocking high pressure cell (Trenberth, 1975; 1979; 1980). The maxima of middle-level cloud variability are evident off the western sides of continents and are generally colocated with the local minima of high-level cloud ability. This middle-level cloud variability pattern is probably caused by the weakening of frontal systems over continents. The pattern of low-level cloud variability in the polar regions follows the wave pattern of climatological mean sea level pressures, indicating the close association between subpolar cyclogenesis and low-level cloud evolution.

5a

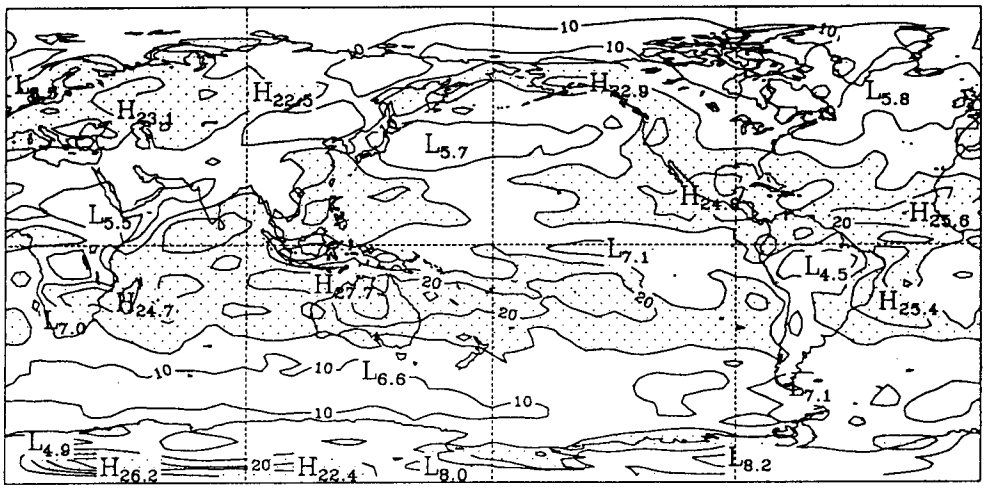

5b

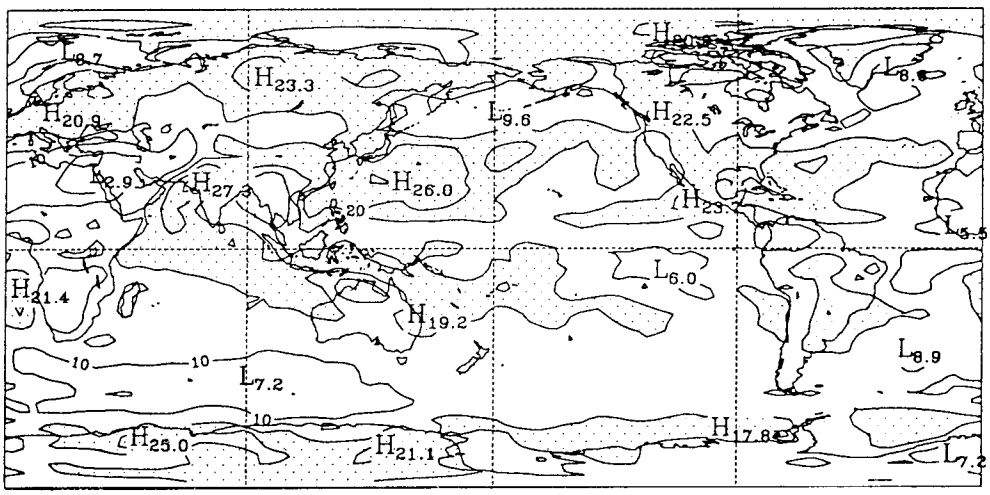

Fig. 5. Band-pass variabilities of observed cloudiness for a) DJF and b) JJA. Values above 15% are stippled.

The contributions of different timescales of cloudiness evolution give an indication of the nature and rates of cloud formation, movement and dissipation. The variability fields of 2.5 - 6 day (or synoptic) bands of total cloudiness for the two seasons are shown in Figures 5a and 5b. Both plots show continuous belts of high variability regions centered at around 35° latitude, reflecting the frontal nature of weather systems in the middle latitudes. Cloudiness variabilities in the Southern Hemisphere are less seasonal, a result of a more uniform underlying surface. The synoptic cloudiness change regimes in the Northern Hemisphere are more seasonal, with high frequency variability becoming less active over the midlatitude continental land masses during summer. The high variability regions in the central Pacific are interesting since they could not be accounted for by frontal movements. Visual examination of daily cloud data showed these regions to be associated with cumulus clusters that sometimes evolve into tropical cyclones. These cloud clusters drift with the prevailing winds but usually dissipate and reform with synoptic scale frequencies. Cloud variability values at high frequencies were also noticeably high over areas with high oceanic/atmospheric temperature contrast, such as those with warm ocean currents in the eastern sides of continents. The major contributors to these high variability values are persistent clouds such as marine stratocumulus which can assume synoptic variability

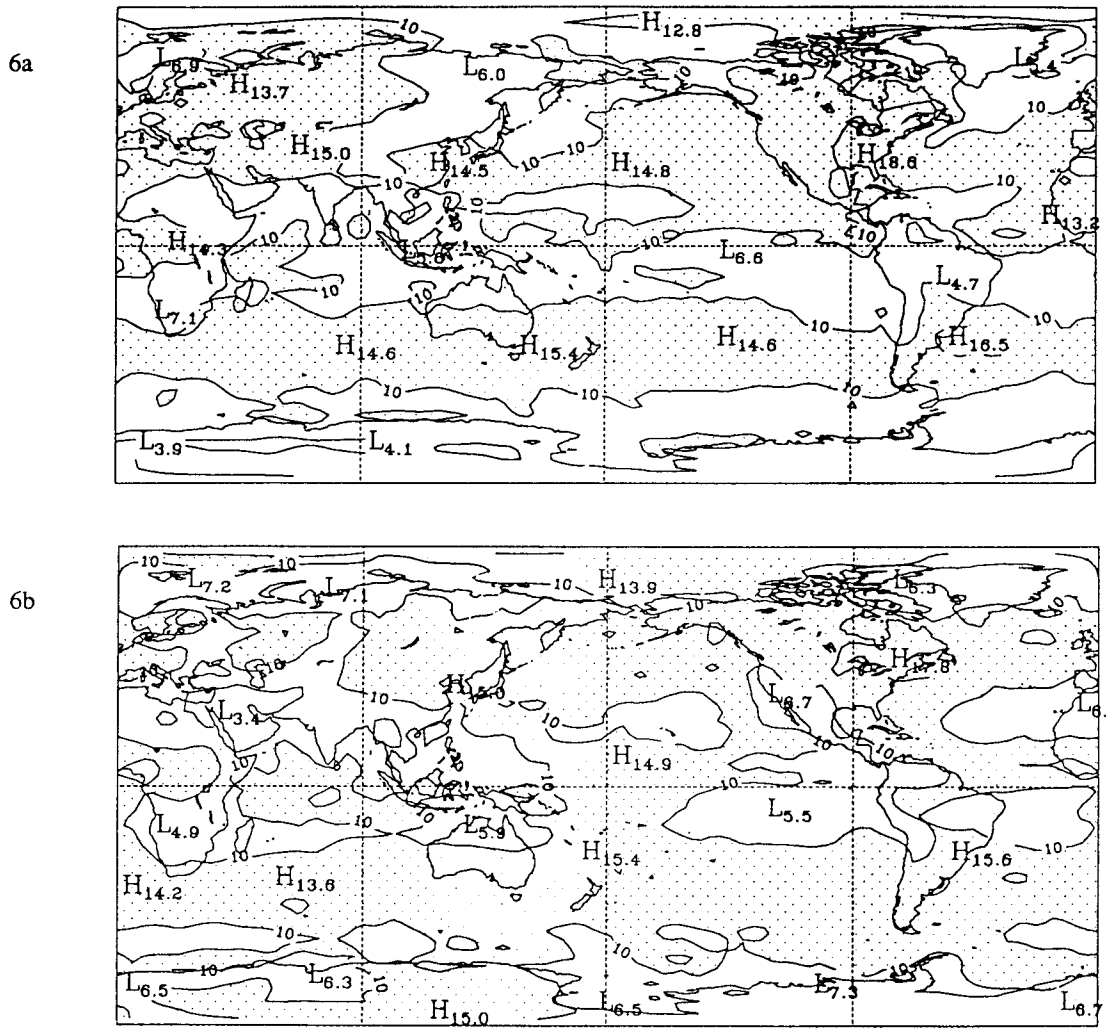

Fig. 6. Low-pass variabilities of observed cloudiness for a) DJF and b) JJA. Values above 10% are stippled.

characteristics with frontal movements. Another factor is the fact that these areas are also cyclone tracks, where tropical cyclones usually lose their tropical characteristics and assume an extratropical nature.

The corresponding cloudiness variability fields for periods greater than 10 days (low pass) are shown in Figures 6a and 6b. Consistently high values of low frequency variabilities are most noticeable over the peripheries of the intertropical convergence zone and the polar fronts, regions that were earlier noted to have low synoptic scale cloud variabilities. This is due to deformations in the semipermanent cloud features in these regions, caused by easterly waves in the tropics, as well as by the long lifespans of ice clouds. The equatorial regions, especially the intertropical convergence zone, have relatively low values of low frequency cloudiness variability. However, cloud variability, by its very nature misses out on near-consistent values of cloudiness amounts. A similar case applies in the climatologically cloud-free regions like the Sahara desert. As in the intertropical convergence zone, the computed cloud variabilities over the Sahara are low for both high and low frequency bands. It is seen from these analyses that cloud variability values have to be used in conjunction with climatological values for the results to be most meaningful.

The geographical distributions of cloudiness variabilities at different cloud levels and at different timescales illustrate the nature of cloud patterns and the processes involved in regional cloud formation. For instance, synoptic scale cloud variabilities are consistently high at all cloud levels at about 75° latitude in the winter hemisphere. These observed synoptic scale cloudiness variabilities reflect the highly synoptic time frame of the undulations of the polar night jetstream. In contrast, the 2.5-6 day variability for high clouds in the lower latitudes exceeds that of middle-level clouds, which in turn, exceeds that of low clouds. One reason for this pattern is the convective nature of cloud formation in the low latitudes. Clouds at the divergent levels of a convection cell are always more extensive than low-level clouds associated with the convergent levels. In addition, cumulonimbus cells which form the bulk of convective cells in the lower latitudes, form and dissipate in periods less than 2.5 days but the associated high-level clouds linger on. From the band-pass variability results, it appears that high-level clouds have a large component which evolves in periods greater than 10 days. The other reason would be the nature of cloud particles. Low-level and middle-level clouds in the low latitudes are predominantly composed of liquid droplets which dissipate faster than ice particles that comprise high-level clouds and clouds at most levels in the high latitudes. This difference in the nature of cloud particles partly explains the large components of low frequency cloudiness variabilities in the polar regions and at high elevations everywhere.

The high and low frequency cloudiness variabilities (or standard deviations) expressed as percentages of the unfiltered cloudiness variabilities are shown in Figures 7 and 8 for DJF and JJA, respectively. This statistic shows the zonal nature of cloud variability since problems associated with absolute variability magnitudes in regions with near-consistent cloud amounts are minimized. The plots confirm the significant contribution of low frequency timescales of cloud variability in the tropics and the high summer latitudes, as well as the seasonal change in high frequency variability contribution favoring the winter middle latitudes. The seasonal changes in variability contributions as explained by the two temporal bands are less pronounced in the Southern Hemisphere and the patterns are more zonally distinct as compared with those of the Northern Hemisphere, most probably due to a difference in the homogeneity of the underlying surface. The higher percentage of total cloudiness variability in the North Pacific is contributed by high frequency modes during winter (DJF) as compared to that during the Northern Hemisphere cyclone season (JJA). This finding may seem contradictory to our statement linking cyclolysis and high frequency cloudiness variability. Although cyclolysis contributes a large part of high frequency cloudiness variability in the North Pacific as can be seen in the JJA case, another regional cloud characteristic is responsible for the observed cloudiness variability in this region during winter. The observed high values of high frequency variability during DJF is

7a

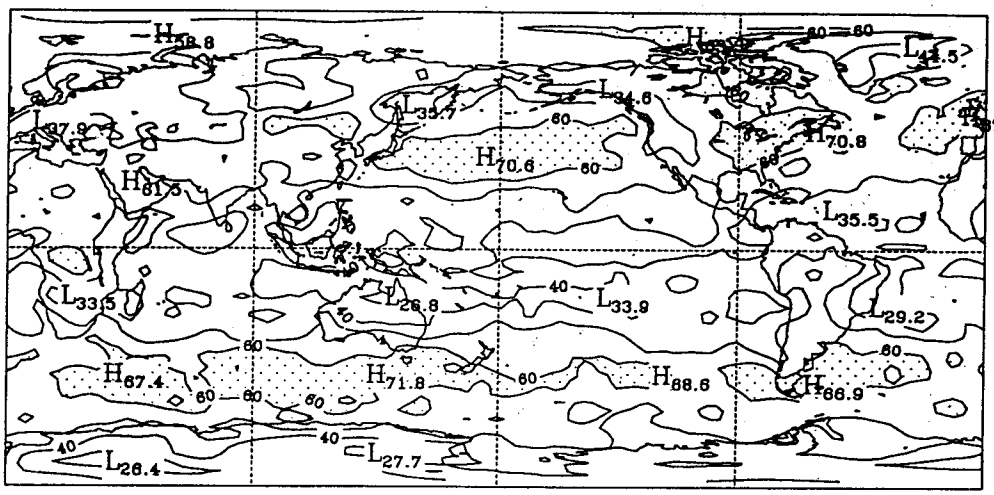

7b

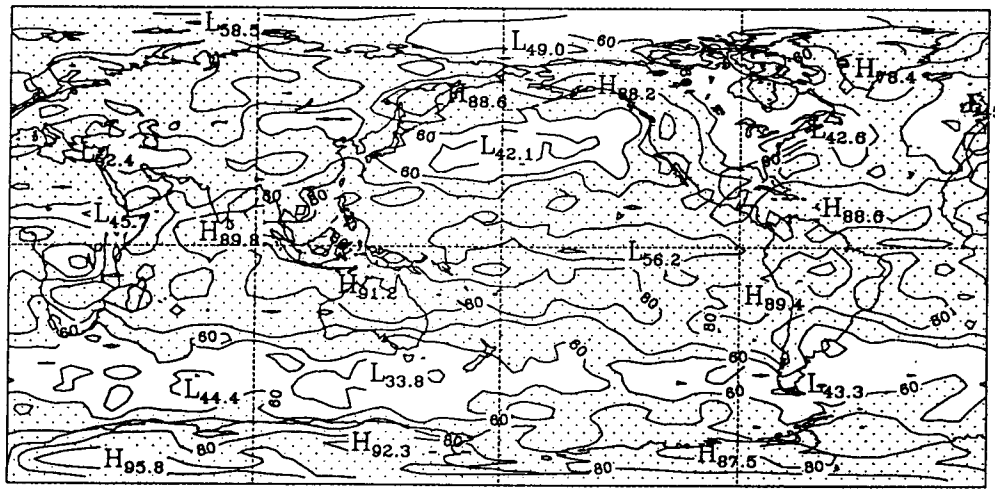

Fig. 7. Percentage of observed total cloudiness variabilities for DJF contributed by a) band-pass and b) low-pass data. Values above 60% are stippled.

primarily due to the greater contribution of northeast cloudbands, which have synoptic scale characteristics and are most predominant in the Northern Hemisphere during the DJF season. In both months, standard deviations explained by high frequency variabilities show bands of high values over Africa. Although this may imply synoptic cloudiness variations, such high values of explained synoptic variabilities were primarily due to the low values of unfiltered variabilities in this region. In general, the variabilities explained by high and low frequency changes are complementary, though non-exclusive, and reflect on the type and nature of predominant clouds in particular regions.

8a

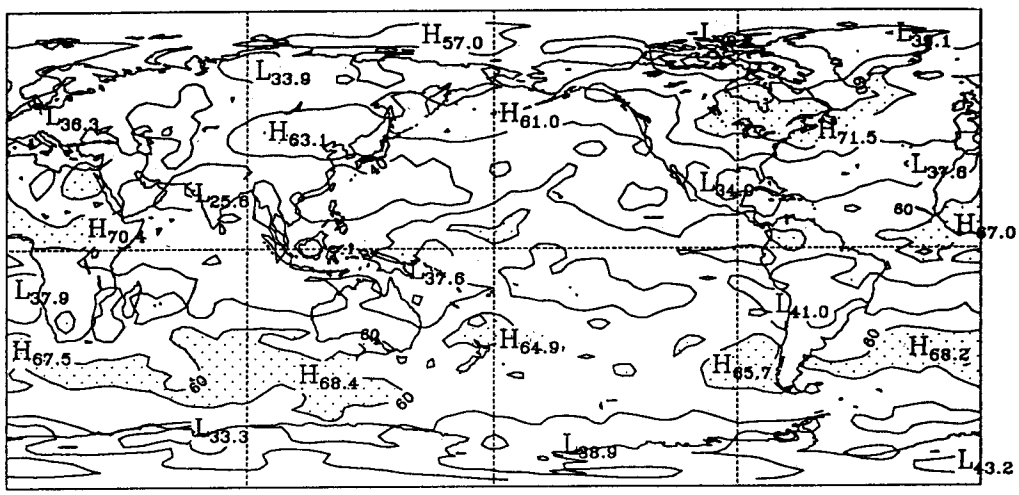

8b

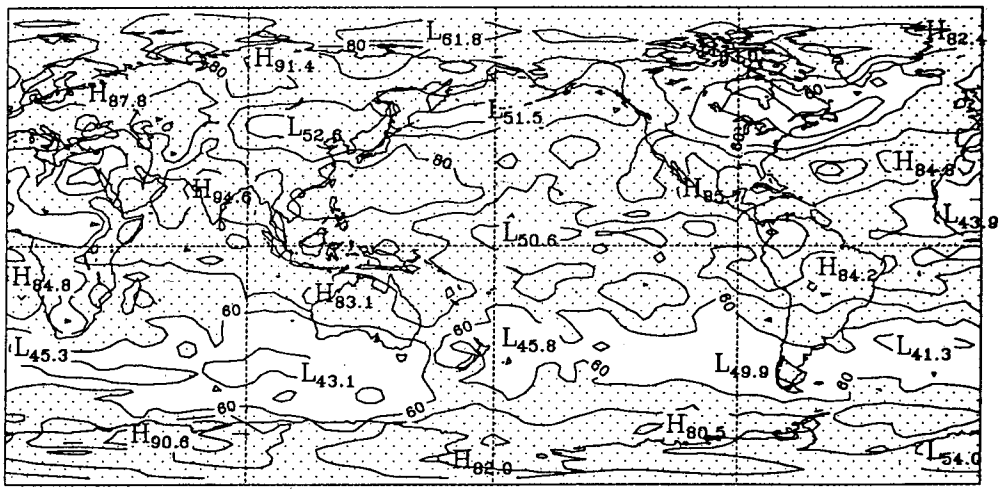

Fig. 8. Percentage of observed total cloudiness variabilities for JJA contributed by a) band-pass and b) low-pass data. Values above 60% are stippled.

5. Modelled temporal variability

Simulations of cloudiness, if they are to be regarded as realistic, must be able to capture both the temporal and spatial structures evident in the observations. The unfiltered variabilities of our model-generated total cloudiness fields for the two months of simulation are shown in Figures 9a and 9b. The structure of the variability fields is simulated reasonably, with low variability in the tropics, high variability over the midlatitude continents, low in the subpolar regions and high variability again in the polar regions simulated with considerable skill. In terms of absolute values, the model overpredicts the unfiltered total cloud variability in comparison with those of observations (Figure 4). This is consistent with the overestimation of variability of model-generated mean sea level pressures in the Southern Hemisphere subpolar regions (Jones and Simmonds, 1993). The systematic overestimation of cloudiness variability in the subpolar regions possibly indicates the presence of strong baroclinicity or the result of deeper troughs

in the Southern Hemisphere subpolar low pressure belts found to be inherent in the GCM, or due to a problem with the cloud scheme itself, in particular the choice of the optimum cloud parameters. Although the climatological values of relative humidity were within the limits of various observational data sets, the aforementioned shortcomings of the model resulted in more severe convective readjustments which were then reflected in the estimates of temporal cloudiness variabilities. The overestimation is also apparent over continental areas, further indicating the link between low surface pressures and cloud formation. Despite this overprediction of modelled total cloudiness variability, the model exhibited overall skill in representing seasonality and in the placement of variability maxima.

9a

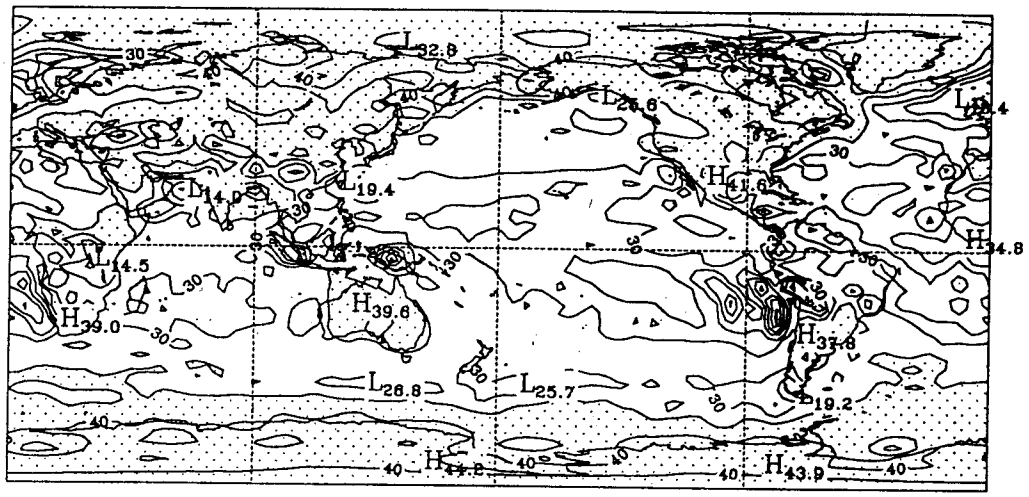

9b

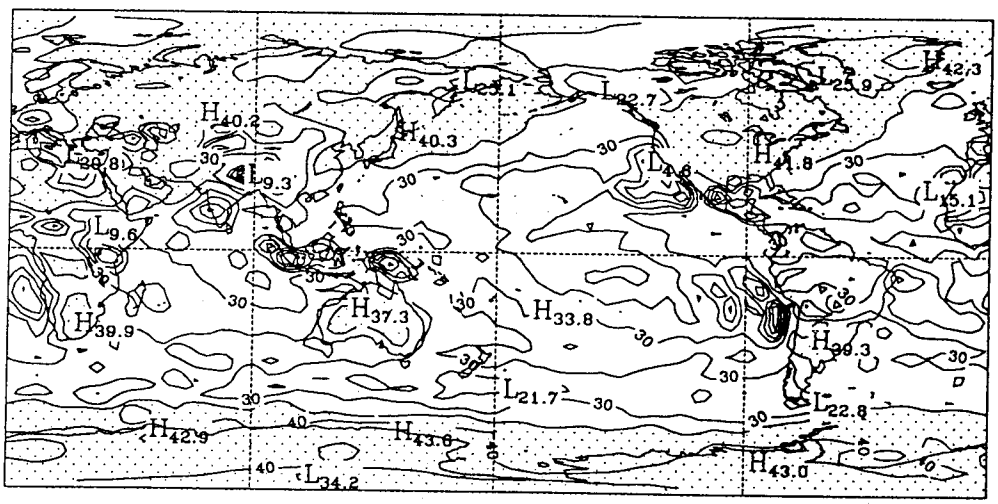

Fig. 9. Unfiltered variabilities of modelled cloudiness for a) January and b) July. Values above 30% are stippled.

Comparison of the variability of clouds at the three levels with the Nimbus-7 data, not shown here for brevity, showed that the modelled cloud variability fields are representative of the observed patterns of high cloud variability maxima in the tropics, middle cloud variability maxima in the middle latitudes, and low cloud variability maxima in the polar regions. The locations of local maxima and minima points are also simulated reasonably well although, again, there is

a systematic overprediction of variability values. The model overprediction was most severe for low-level and high-level clouds and for clouds at all levels in the polar regions. Aside from the causes listed so far, other causes of these shortcomings are varied: for low-level clouds in the lower latitudes, the computed high variabilities maybe due to the model not adequately representing persistent surface processes like surface moisture flux, for high clouds and in high latitudes, the overprediction of cloudiness variabilities is due to the non-representation of ice clouds. Basically, the cloud parameterization scheme does not specify the nature of cloud particles, hence their residence times. Considering these findings, it is highly desirable for improvements in large-scale cloud parameterization to incorporate this aspect of cloudiness.

10a

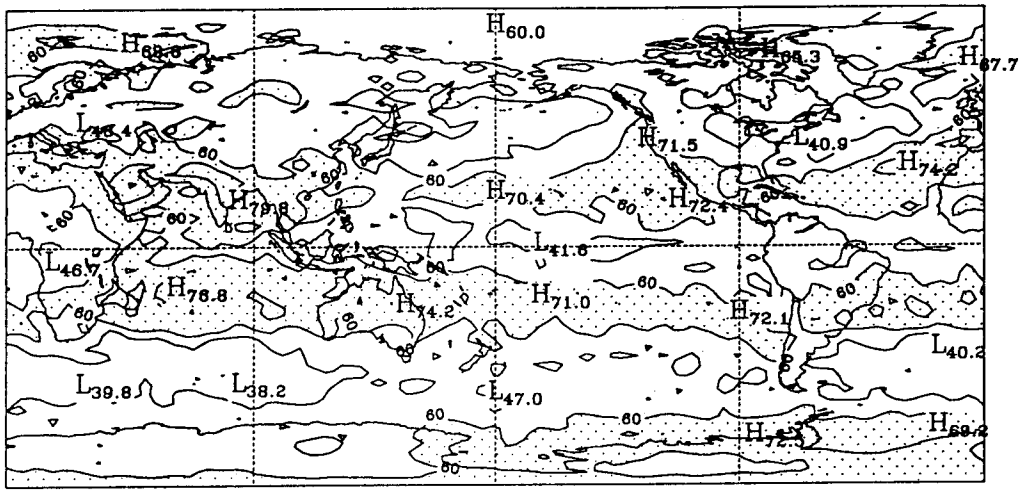

10b

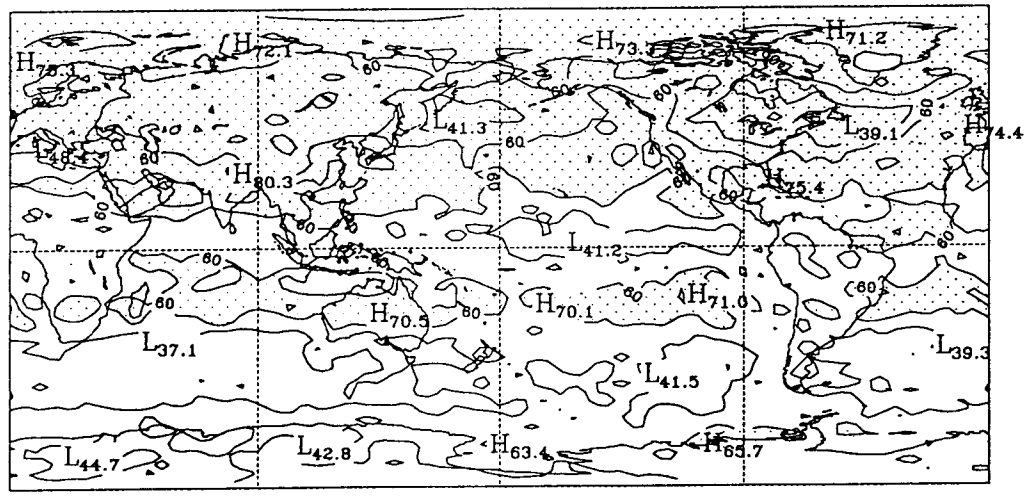

Fig. 10. Percentage of modelled cloudiness variabilities contributed by band-pass mode for a) January and b) July. Values above 60% are stippled.

As in the analysis of observed cloudiness data, the variability patterns of model-generated cloudiness show more coherence when presented as percentage contributions of low-pass and band-pass variabilities to the total. Figure 10 shows the 2.5 - 6 day variability contributions to the total variability for the January and July cases, respectively, while Figure 11 shows the

corresponding contributions of frequencies greater than 10 days. Comparisons with observations showed that the model correctly predicted the higher contribution of low-pass variability in the subtropics at about 20° latitude and near the summer poles, and the higher contribution of band-pass variability in the middle latitudes and around the winter poles. The zonal nature of the relative contributions of different variability periods is apparent in the model simulations, though not as distinct as in the observed data. The biggest discrepancies between observed and modelled cloudiness variabilities were those for low-pass values over Antarctica. The model underpredicted low frequency cloudiness variabilities over the southern polar regions in both seasons. In contrast, the model slightly overpredicted synoptic scale cloudiness variabilities over most of the middle and low latitudes. Considering the higher unfiltered variability values of model results, it is quite likely that cloudiness variability periods shorter than 2.5 days are also active in the model.

11a

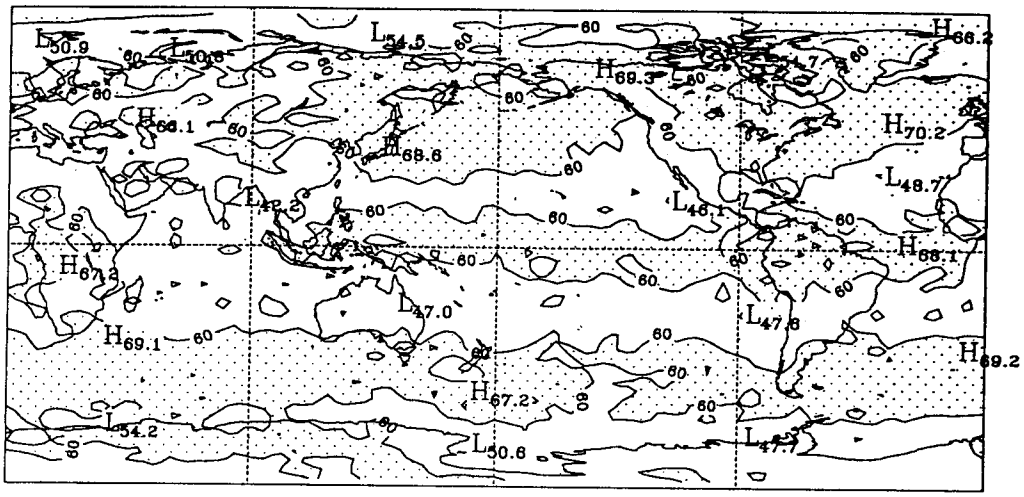

11b

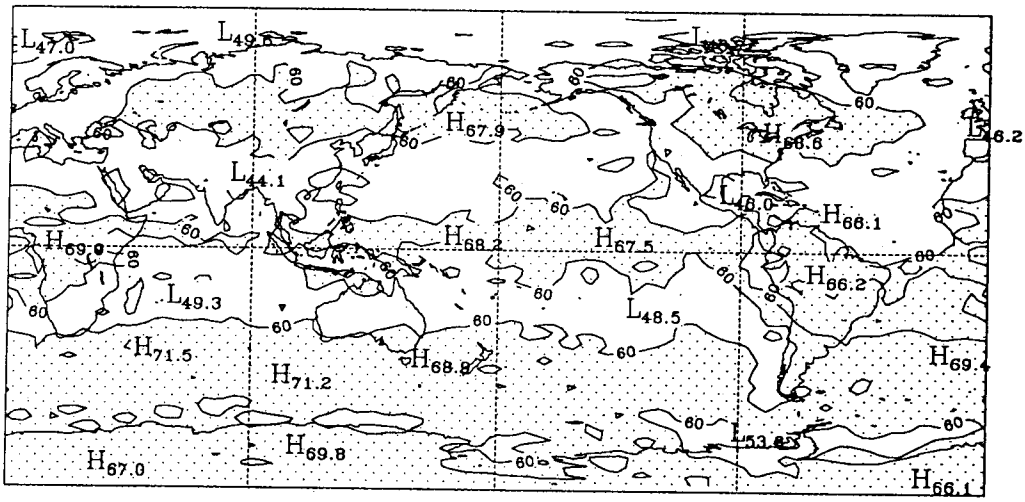

Fig. 11. Percentage of modelled cloudiness variabilities contributed by low-pass model for a) January and b) July. Values above 60% are stippled.

Another way of considering the time evolution or variability of cloudiness is to look at the time section of cloudiness values at a particular latitude. A display of this nature has been presented in Figure 12 for the observations (JJA 1980) and the model for 9°N, the mean July position of the Intertropical Convergence Zone. In this form, a pattern of temporal cloud structure can be clearly seen, particularly with reference to its longitudinal dependence. Observed total cloudiness for the 92-day period of JJA 1980 is compared with a 92-day model-generated total

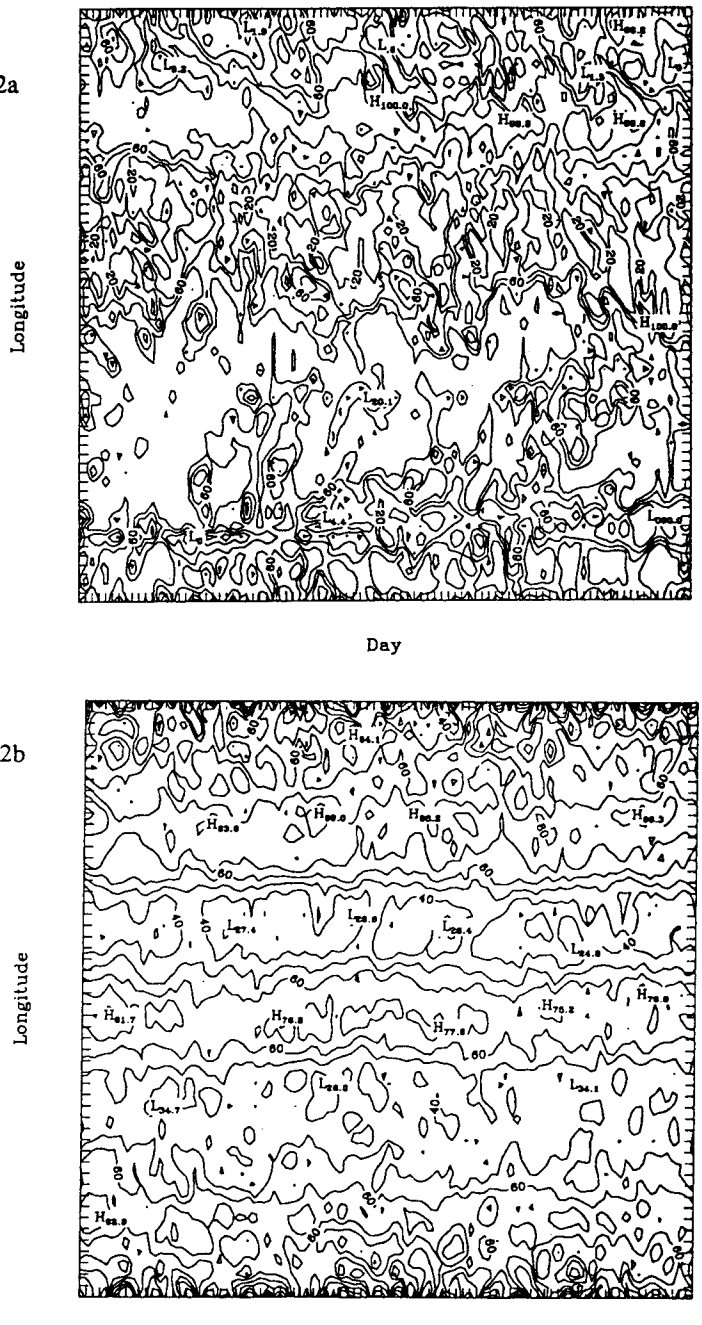

Fig. 12. Time section of total cloudiness at 9°N for July 1980 and JJA from a) Nimbus-7 observations and b) GCM simulation, respectively.

cloudiness trend from the July simulation starting from day 200. Because the model has been run for a long period, we are not looking for correspondence between the two plots; rather we simply wish to comment on the structures. The cloud amounts are given in percent with a contour interval of 20%. Since the method was applied to the tropical regions, the time section or Hovmoller diagram clearly shows the structure of the Walker circulation, with high cloudiness values in areas associated with ascending air and vice versa. Modelled cloudiness amounts are consistently high over the convergent regions of the Walker cell namely, over equatorial Africa, the Indonesian archipelago and the Amazon, and consistently low over the oceanic regions. The direction of cloud movement in the model is not very clear, although there are indications of eastward-moving cloud clusters embedded within larger westward-moving cloud masses in the observational data, similar to the findings of Nakazawa (1988) and Lau *et al.* (1991). The slopes of both eastward- and westward-moving cloud masses indicate a propagation speed of about 10 m/sec.

6. Concluding remarks

In this study, the global distributions of temporal mean and variability statistics of six years of daily cloudiness data are examined. The ability of a GCM to simulate this range of statistics is then assessed. By analyzing the observed patterns, the temporal characteristics of global cloudiness can be seen in terms of the causal factors. Such an understanding should help in evaluating the ability of the cloudiness parameterization scheme, and the GCM, in simulating atmospheric processes. The analyses of daily variability of observed cloudiness showed naturally occurring variabilities as high as 31%. The patterns of cloud variability are noticeably zonal, with variability maxima usually occurring in regions with high climatic extremes. Semiarid regions like sub-Saharan Africa, Australia, the southern parts of North America, central Asia and eastern South America fitted this description. Arid and humid regions generally have low cloudiness variability, implying semiperpetual clear or cloudy conditions. The lowest cloud variability values were located over the desert regions of the Middle East and Sahara, as well as the regions affected by the Indian monsoon. High values of cloud variability over oceanic areas correspond with regions of cyclogenesis and tropical cyclone tracks. The cloud variability signature of extratropical cyclones, especially over the Southern Oceans, was masked by the natural cloud variability in the subpolar low pressure zones.

Some characteristic cloudiness patterns are inherently associated with cyclones. This association has always been utilized in the visual tracking of tropical cyclones from satellite imageries. It would appear from the results of cloud variability analyses that the determination and analysis of cyclone density in the high latitudes are better done using other quantities like mean sea level pressure as the prognostic variable. Cloudiness variability as a measure of cyclonic activity in the baroclinically active latitudes can be misleading considering the naturally high cloudiness variability associated with these regions. However, cloud variability seems to be more appropriate in the determination of cyclone density in the low latitudes, in contrast to mean sea level pressure variability which has been found to be underestimated in the tropics by the model.

The generated cloud fields from the two perpetual-month climate simulations correctly placed the regions of cloud variability extrema, with the greatest skill observed in the low and middle latitudes. The simulated cloudiness variability in the high latitudes are considerably overestimated, suggesting a strong link between cloud evolution and high-level winds. These winds have been shown to be overestimated in the model, primarily due to high temperature gradients near the poles. The indirect result of these anomalous wind velocities in the model is poor simulation of cloud drift. In terms of cloud variability, the presence of fast moving cloud masses, together with the instantaneous nature of model cloud formation (which is not always true especially

for ice clouds) results to the modelled cloud variability being biased towards the high frequency modes. A possible solution would be to incorporate cloud residence time as a function of cloud temperature and thickness. Such an approach could possibly remedy the deficiency in cloud drift and bring the modelled cloudiness values still closer to the fidelity of the Nimbus-7 data.

REFERENCES

Blackmon, M. L. and N. C. Lau, 1980. Regional characteristics of the Northern Hemisphere wintertime circulation: A comparison of the simulation of a GFDL General Circulation Model with observations. *J. Atmos. Sci.*, **37**, 497-514.

Bishop, J. K. B. and W. B. Rossow, 1991. Spatial and temporal variability of global surface irradiance. *J. Geophys. Res.*, **96**,(C9), 16839-16858.

Charlock, T. P., K. Kondratyev, and M. Prokofyev, 1993. Review of recent research on the climatic effects of aerosols. University of Arizona Press, In: Aerosol Effects on Climate, Jennings, S.G. (ed.), 233-274.

Geleyn, J. F., 1981. Some diagnostics of the cloud-radiation interaction in ECMWF forecasting model. In: Proc. ECMWF Workshop on Radiation and Cloud-Radiation Interaction in Numerical Modelling, 135-162.

Gent, P. G. and J. J. Tribbia, 1993. Simulation and predictability in a coupled TOGA model. *J. Climate*, **6**, 1843-1858.

Hahn, C. J., S. G. Warren, J. London, R. L. Jenne, and R. M. Chervin, 1988. Climatological data for clouds over the globe from surface observations. NDP026, Carbon Dioxide Information Analysis Center.

Hughes, N. A., 1984. Global cloud climatologies: An historical review, *J. Climate and Appl. Meteorol.*, **23**, 724-751.

Jones, D. A. and I. Simmonds, 1993. Time and space spectral analyses of Southern Hemisphere sea level pressure variability. *Mon. Wea. Rev.*, **121**, 661-672.

Kasahara, A. and W. M. Washington, 1971. General circulation experiments with a six-layer NCAR model, including orography, cloudiness and surface temperature calculations. *J. Atmos. Sci.*, **28**, 657-700.

Katz, R. W., 1983. Procedures for determining the statistical significance of changes in variability simulated by an atmospheric general circulation model. Rep. No. 48, 23 pp.

Kvamsto, N. G., 1991. An investigation of diagnostic relations between stratiform fractional cloud cover and other meteorological parameters in numerical weather prediction models. *J. Appl. Meteorol.*, **30**, 200-216.

Morcrette, J. J. and Y. Fouquart, 1986. The overlapping of cloud layers in shortwave radiation parameterization. *J. Atmos. Sci.*, **43**, 321-328.

Morcrette, J. J., 1991. Evaluation of model-generated cloudiness: satellite-observed and model-generated diurnal variability of brightness temperature. *Mon. Wea. Rev.*, **119**, 1205-1224.

Nakazawa, T., 1988. Tropical super clusters with intraseasonal variations over the western Pacific. *J. Meteor. Soc. Japan*, **66**, 823-839.

Ricketts, J. N. 1973. An investigation into a relationship between upper-air relative humidity and cloud cover. *Met. Mag.*, **102**, 146-153.

Saito, K. and A. Baba, 1988. A statistical relation between relative humidity and the GMS observed cloud amount. *J. Meteorol. Soc. Japan.*, **64**, 187-192.

Sasamori, T., 1975. A statistical model for stationary atmospheric cloudiness, liquid water content, and rate of precipitation. *Mon. Wea. Rev.*, **103**, 1037-1049.

Schneider, S. H. and R. E. Dickinson, 1976. Parameterization of fractional cloud amounts in climatic models: The importance of modeling multiple reflections. *J. Appl. Meteorol.*, **15**, 1050-1056.

Simmonds, I., 1985. Analysis of the 'spinup' of a general circulation model. *J. Geophys. Res.*, **90**, 5637-5660.

Simmonds, I., G. Trigg, and R. Law, 1988. The climatology of the Melbourne University GCM. Publication No. 31, Department of Meteorology, University of Melbourne, 67 pp.

Slingo, J. M., 1985. Parameterization of cloud cover. In: Proc. ECMWF Symposium on Physical Parameterization for Numerical Models of the Atmosphere, 17-46.

Slingo, J. M., 1987. The development and verification of a cloud prediction scheme for the ECMWF model. *Q.J.R. Meteorol. Soc.*, **113**, 899-927.

Slingo, J. M., K. R. Sperber, J. J. Morcrette, and G. L. Potter, 1992. Analysis of the temporal behavior of tropical convection in the ECMWF model. PCMDI Rep. No. 2.

Soden, B. J., 1992. Validation of cloud forcing simulated by the NCAR CCM using observations from ERBE. *J. Geophys. Res.*, **97**. 18137-18159.

Stowe, L. L., H. Y. M. Yeh, T. F. Eck, C. G. Wellemeyer, and H. L. Kyle, 1989. Nimbus-7 global cloud climatology. Part II: First year results. *J. Climate*, **2**, 671-709.

Tian, L. and J. A. Curry, 1989. Cloud overlap statistics. *J. Geophys. Res.*, **94**, 9925-9935.

Tiedtke, M., 1985. Effect of physical parameterization on the large-scale flow in the ECMWF model. In: Proc. ECMWF Seminar on Physical Parameterization for Numerical Models of the Atmosphere, 277-314.

Trenberth, K. E., 1975. A quasi-biennial standing wave in the Southern Hemisphere and interrelations with sea surface temperatures. *Q.J.R. Meteorol. Soc.*, **101**, 55-74.

Trenberth, K. E., 1979. Interannual variability of the 500mb zonal mean flow in the Southern Hemisphere. *Mon. Wea. Rev.*, **107**, 1515-1524.

Trenberth, K. E., 1980. Planetary waves at 500mb in the Southern Hemisphere. *Mon. Wea. Rev.*, **108**, 1378-1389.

Warren, S. G., C. J. Hahn, J. London, R. M. Chervin, and R. L. Jenne, 1986. Global distribution of total cloud cover and cloud type amounts over land. NCAR Technical Note TN-273+STR.

Weare, B. C., 1992. Variations in Nimbus-7 cloud estimates. Part I: Zonal averages. *J. Climate*, **5**, 1496-1505.

Xu, K. M. and S. K. Krueger, 1991. Evaluation of cloudiness parameterizations using a cumulus ensemble model. *Mon. Wea. Rev.*, **119**, 342-367.

Yu, W., G. Seze, H. LeTreut, and M. Desbois, 1991. Comparison of radiance fields observed by satellite and simulated by the LMD general circulation model. *Dyn. Atmos. and Oceans*, 61.